OPEN ACCESS
IOP Publishing
Superconductor Science and Technology
Supercond. Sci. Technol. **38** (2025) 075023 (15pp)
https://doi.org/10.1088/1361-6668/aded3b

Tape-in-tape-out (TITO): a new approach for *in-situ* contact resistance measurements in high temperature superconducting CORC® cables

Reed Teyber[1,*], Chet L Spencer[1], Jeremy Weiss[2,3] and Danko van der Laan[2,3]

[1] Lawrence Berkeley National Laboratory, Berkeley, CA 94720, United States of America
[2] Advanced Conductor Technologies LLC, Boulder, CO 80309, United States of America
[3] Department of Physics, University of Colorado, Boulder, CO 80309, United States of America

E-mail: rteyber@lbl.gov

Received 16 April 2025, revised 17 June 2025
Accepted for publication 8 July 2025
Published 21 July 2025

Abstract

One of the ongoing development challenges with ReBCO high-temperature superconducting (HTS) cables is normal zone initiation and local heating, which is associated with over-critical current flowing through and around local performance reductions in individual tapes. Although inter-tape contact resistances are well-reported for individual tapes and HTS cables, these measurements are a challenge in CORC® cables as current percolates through much of the cable. In this work, developments in tape-in-tape-out (TITO) automated individual tape powering experiments are presented, and a simplified modeling approach for current percolation in CORC® cables is developed. An optimization is formulated to fit the model parameters to a large set of TITO experiments on a single cable, allowing the layer-dependent inter-tape contact resistance to be extracted. Measurements are presented and discussed for a straight CORC® cable and a cable bent to a 152 mm and 76 mm radius. The approach provides both quantitative insight and facilitates better understanding of current sharing phenomena in HTS cables.

Supplementary material for this article is available online

Keywords: high temperature superconductor, ReBCO, CORC®, contact resistance, current sharing

* Author to whom any correspondence should be addressed.

1. Introduction

ReBCO high temperature superconducting cables [1–4] have the potential to push the performance limits of fusion and high energy physics magnets [5]. Some of the ongoing development challenges include conductor stability caused by local performance reductions in individual tapes from tape manufacturing, magnet manufacturing and magnet operation [6–11]. Current redistribution around local defects can induce a magnet quench and irreversible performance degradation. A theme in our research [12–14] is that knowledge of defects and cable parameters (such as termination resistances and inter-tape contact resistances) could ultimately be used as inputs to simulation tools that guide safe operation specific to individual magnets [12]. This would also enable the implementation of reduced-cost high-temperature superconducting (HTS) cables wound from variable performance tapes [15]. Although challenging to realize, such a regime requires new *in-situ* methods to extract cable-specific parameters of HTS cables. The use of cable-specific models to predict current distributions in real time is being explored as a quench detection methodology [13, 16, 17].

Van der Laan *et al* (2024) [18] recently published *I*–*V* curves of CORC® cables bent to various radii, after which tapes were sequentially extracted and individually characterized. Although high bending performance is ultimately achieved, the extracted tape measurements show a complex radial distribution of tape performance in HTS cables bent to their limit (see Anvar *et al* (2018) [19]). Extracted tape measurements provide the best data for simulating and informing safe magnet operation, however doing so *in-situ* or non-destructively is a challenge.

Phifer (2023) [20] presented a Hall sensor-scanning device for identifying anomalous magnetic fields around defects in CORC® cables, and Lai *et al* (2025) [21] recently presented numerical and experimental results for their own Hall sensor-based cable defect scanning device. Although promising results were reported by both authors, it can be challenging to dis-aggregate the local current distribution from the complex screening currents [22] in high tape and layer count cables [23]. Teyber *et al* (2022) [14] presented a two-axis permanent magnet Halbach [24] cable scanning device, and the location, angle and magnitude of cable defects were identified from 10 500 automated *I*–*V* curves.

The *in-situ* measurement of inter-tape resistance in CORC® cables is a key parameter driving current sharing and local heating around performance limiting regions, and it has been investigated in literature for both tapes [25–27] and cables. Yagotintsev *et al*(2020) [28] presented individual tape powering experiments in a variety of HTS cables, and reported varying inter-tape contact resistances between outer and inner layers of a CORC® cable. Phifer *et al* (2022) [29] presented experimental measurements of the inter-tape contact resistivity in straight and bent CORC® cables. A variety of winding lubricants and tape coatings (e.g. solder-coated) are also investigated, along with microscopy of the cable cross sections.

In CORC® tape-in-tape-out (TITO) individual tape powering experiments, current flow occurs in a complex percolation network, complicating the interpretation of inter-tape resistances. In this work, we develop a TITO experiment with voltage tap arrays in combination with automated high current tape switching and perform measurements on a cable that is straight and sequentially bent to a 152 mm and 76 mm radius. A fast TITO simulation tool is developed, enabled by neglecting the impact of the copper core, and an optimization is formulated for dis-aggregating the individual tape resistances from the percolating current distribution in the cable. Our approach is able to measure the intrinsic inter-tape contact resistance and probe current sharing behaviors in CORC® cables.

2. Methods

2.1. TITO experiments

Figure 1 shows the developed TITO terminations (bottom left), where each tape in a layer is mechanically supported by a G10 plate and connected to a conductive braid and voltage tap. A single CORC® cable is investigated in this work as shown in figure 1 and summarized in table 1. This 0.9 m long CORC® cable has a total of 12 tapes of 4 mm width, with four layers and three tapes per layer.

Current is injected and extracted on the same side of the cable (i.e. cable has a TITO termination on one end and is free on the other). This is based on the assumption that at low currents, resistive current sharing effects dominate and any superconducting voltage is negligible. This is described in more detail in the percolation model description below. This single-ended current injection and extraction simplifies the electrical controls, reduces the number of individual tape terminations, and facilitates the ability to perform measurements while bending the cable to various radii. In this work, the cable is characterized straight and bent to radii of 152 mm and 76 mm (see figure 1). A bending fixture was fabricated consisting of stacked 3/8" tall plastic cylinders of the desired bending radii. The sample was hand-held by the cable (not termination), and with the other hand the sample was progressively wrapped around the cable bending fixture in a wiping left-to-right motion.

Two developments were prioritized in the TITO individual tape powering experiments; automated experiments (tape switching, powering and data acquisition of tape combinations), and measurement of all tape voltages for each experiment. The automated TITO test setup is depicted in figure 2. High and low side MOSFET switch boards were fabricated for liquid nitrogen operation, part of which are seen in the top right of figure 1. Layers 0 and 2 interface to the positive switch network, and layers 1 and 3 interface to the negative switch network and power supply ground. This allows all neighboring tape combinations to be tested, as well as the

Table 1. Cable parameters assumed in model.

Parameter	Value
w_{tape}	4 [mm]
L_{cable}	900 [mm]
P_{avg}	21.4 [mm]
n_{turns}	42 [−]
r_{avg}	2.8 [mm]
n_{tape}	12 [−]
n_{layer}	4 [−]
ρ_{tape}	3 [tape/layer]

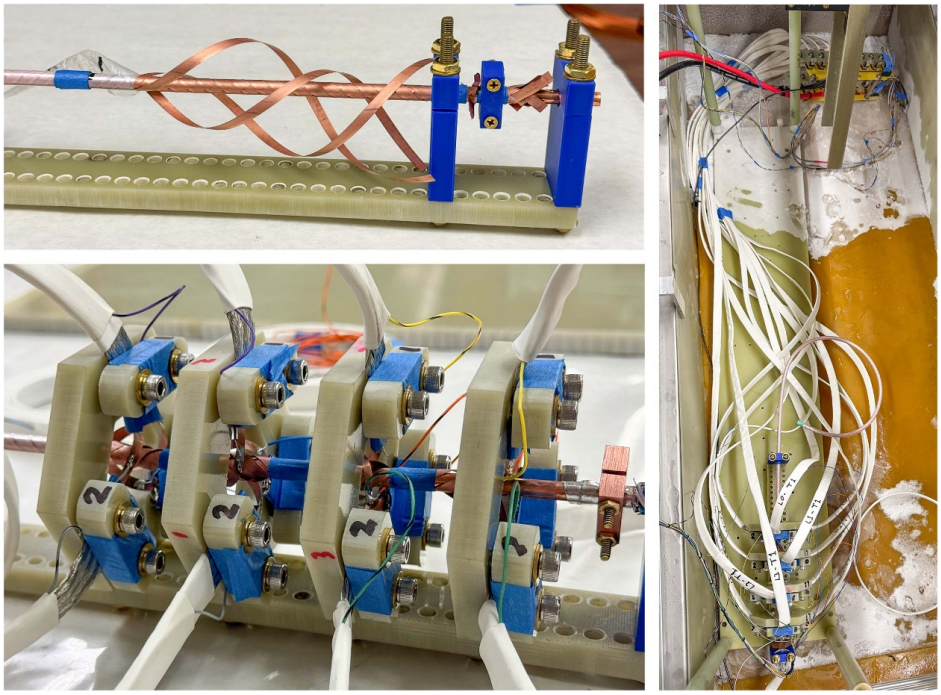

Figure 1. (Top left) Un-furling the CORC® outer layer. (Bottom left) The TITO termination, showing braided cable and a voltage tap connecting to each of 12 supported tapes. (Right) The TITO experiments, showing the cryo switch network (top) and the cable bent to a 76 mm radius.

outer-most and inner-most layers, while avoiding the implementation complexity of allowing each tape to be switched to either the high or ground side of the power supply. The white lines show the current percolation paths through the cable.

Infineon IRLB 3813 MOSFETS were used which have a measured on resistance of 1 mΩ at 77 K and a gate voltage of 12 V. The 12 V MOSFET gate voltage is controlled by a USB relay board with a python (i.e. serial) interface, which also communicates with a 200 A power supply and 24 bit National Instruments data acquisition cards. The voltage of each tape is measured with respect to a common voltage tap on the ground lead, and all measurements are digitally scaled to force the output tape to 0 V.

2.2. Percolation model

A central goal of this manuscript is to extract the inter-tape contact resistance of a CORC® cable as a function of cable layer, and to probe how the magnitude and distribution of contact resistance changes as a cable is manipulated (i.e. bent). Since current percolates through many tapes neighboring the input and output pair, a predictive tool is required to disaggregate the local inter-tape resistance from this global behavior. This section describes the current percolation model that was developed to simulate TITO experiments. The subsequent section describes our optimization approach to extract cable current sharing parameters using the percolation model and experimental TITO results.

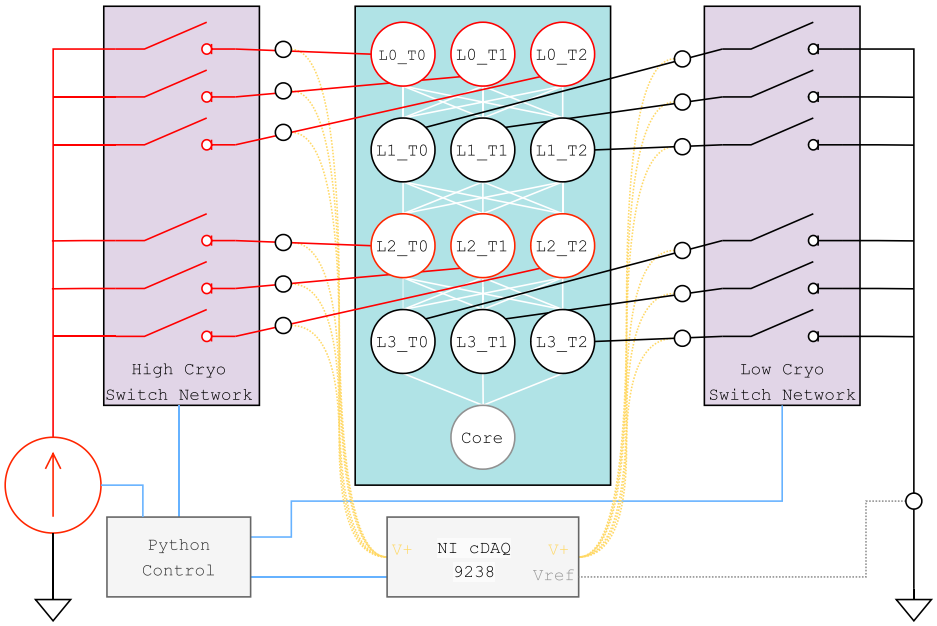

Figure 2. Automated TITO experiments. Each circle represents a single tape in the CORC® cable

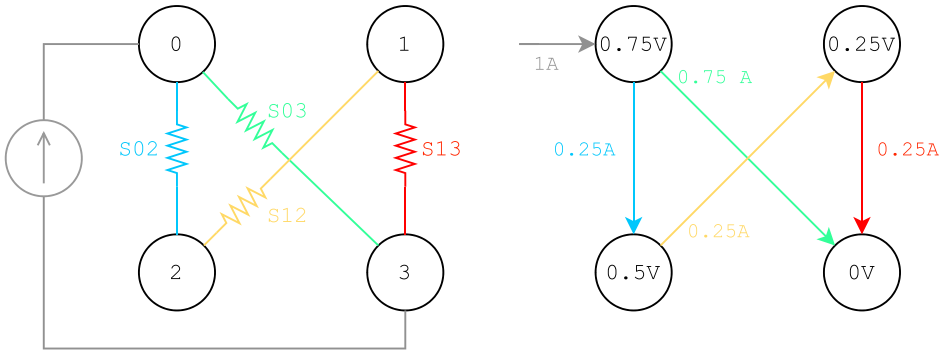

Figure 3. Simplified configuration for resistive percolation model (left). Voltage and current distribution for uniform conductance $S_{ij} = 1$, $I_{\text{transport}} = 1$ (right).

When transport currents are low, the cable current distribution in a TITO experiment is governed by resistive current sharing behavior and each tape is equipotential along the tape length. If the copper core is neglected, the traditional HTS cable modeling problem [12] simplifies to finding the single voltage of each tape in a linearly resistive network. The CORC® cable can then be visually un-wrapped as shown in figure 2. Although there are scenarios where the copper core should not be ignored, this simplifying assumption is key to enabling our fast TITO simulation methodology. The percolation model is formulated here for the trivial 4-tape CORC® TITO experiment in figure 3, however all experimental and numerical results in this manuscript are with the 12-tape cable of table 1. In figure 3, current is injected into node 0 and extracted from node 3. Nodes 0 and 1 are in the same layer (no contact), and nodes 2 and 3 are in the same layer.

The resistance between tapes $i-j$ is calculated from the average contact resistivity and area over the length of each tape, and the conductance (S_{i-j}) is the inverse of the resistance.

$$S_{i-j} = 1/R_{i-j} = \frac{A_{i-j}\,[m^2]}{R_{\text{ct}}\,[\Omega - m^2]} \tag{1}$$

A current balance at each node in figure 3 yields the following system of equations

$$\begin{aligned} I_{\text{transport}} + S_{02}\,(V_2 - V_0) + S_{03}\,(V_3 - V_0) &= 0 \\ S_{12}\,(V_2 - V_1) + S_{13}\,(V_3 - V_1) &= 0 \\ S_{02}\,(V_0 - V_2) + S_{12}\,(V_1 - V_2) &= 0 \\ -I_{\text{transport}} + S_{03}\,(V_0 - V_3) + S_{13}\,(V_1 - V_3) &= 0 \end{aligned} \tag{2}$$

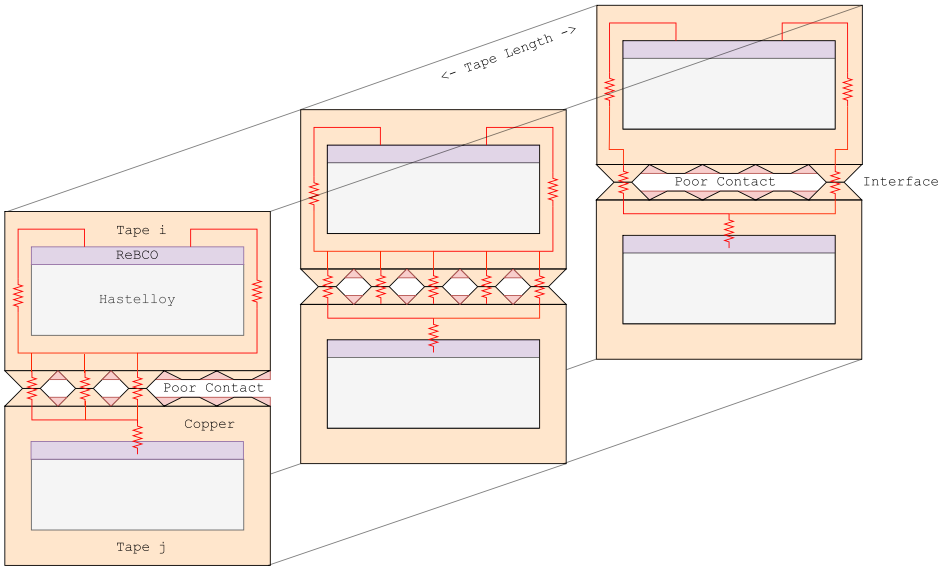

Figure 4. Illustration of the resistance network between superconducting ReBCO layers in a two tape stack.

or in matrix form

$$\begin{bmatrix} -(S_{02}+S_{03}) & 0 & S_{02} & S_{03} \\ 0 & -(S_{12}+S_{13}) & S_{12} & S_{13} \\ S_{02} & S_{12} & -(S_{02}+S_{12}) & 0 \\ S_{03} & S_{13} & 0 & -(S_{03}+S_{13}) \end{bmatrix} \times \begin{bmatrix} V_0 \\ V_1 \\ V_2 \\ V_3 \end{bmatrix} = \begin{bmatrix} -I_{\text{transport}} \\ 0 \\ 0 \\ I_{\text{transport}} \end{bmatrix} \tag{3}$$

which can be inverted to find the voltage of each node. The output tape is prescribed as the ground (here $V_3 = 0$) and is eliminated from the system before solving. Once the voltage distribution is solved, the current between any two tapes $i-j$ can be calculated from the voltage difference and S_{i-j}. With uniform $S_{i-j} = 1$ and $I_{\text{transport}} = 1$, the resulting voltages are $V_0 = 0.75$, $V_1 = 0.25$, $V_2 = 0.5$ and $V_3 = 0$ as shown on the right of figure 3. Although the transport current is 1 A, the current flowing directly between the input and output tape is $I_{0-3} = 0.75$ A, with the remaining 0.25 A flowing from 0–2 to 2–1 to 1–3. This percolation effect is exacerbated in higher tape cables, and this simple example illustrates the need to consider the bulk cable in TITO experiments for measuring inter-tape contact resistance.

The percolation model takes the cable geometry and average inter-tape contact resistance per unit area as inputs. The contact area is calculated using the approach in Teyber *et al* (2022) [12] with the cable parameters in table 1. With this twelve-tape cable, the variation in radius and winding pitch between the four layers is neglected, and average values are used instead. For our cable, this simplification under-reports the tape area in the inner-most layer by 4% and over-reports the tape area in the outer-most layer by 4 %. The approach also assumes that the tapes are in intimate contact over the entire cable length, and any gaps or local reductions in contact area will result in an increase in extracted resistance.

Although the inter-tape contact resistance is often associated with asperities formed by the surface roughness of two mating surfaces [25, 27, 30], figure 4 illustrates how the inter-tape contact resistance is formed by a more complex resistive network. For the 12 tape cable in figure 2, there are 27 unique experimental pairs which result in a contact resistance matrix defined by 27 parameters. In the absence of tape defects, we assume that a single tape pair will not exhibit an anomalous contact resistance—in figure 2, we would not expect to measure uniform contact resistances in the first 26 of 27 TITO pairs and an elevated contact resistance in the final TITO pair L2 T2 - L3 T2. We use this reasoning to motivate our simplified approach of modeling the 12 tape cable with 12 contact resistance parameters instead of 27 parameters, which facilitates our optimization process described in section 2.3 below. The inter-tape resistance between two tapes is the sum of the reported resistances of each tape (see figure 7 and table 3). It should be emphasized that this approach does not neglect the interface resistance, it lumps the interface resistance into the individual tape resistances in a least-squares sense.

Some of the results show anomalous voltages at only the input or output tapes. If a performance reduction (e.g. superconductor dropout) exists inside the cable, the percolation model assumptions are challenged and a higher fidelity HTS cable modeling tool is needed. If a performance reduction is outside the cable in the termination, it can be handled in the percolation model via the inclusion of a termination resistance. Once the percolation model is solved, the voltage of a tape node with non-zero termination resistance is simply shifted by $R_{\text{term}} I_{\text{transport}}$.

2.3. Optimization for contact resistivity extraction

The TITO experiments yield the voltage distribution in the CORC® cable as a function of current for all input–output combinations specified in figure 2. The percolation model described above takes any input termination resistances and the 12 inter-tape resistances, which is the contribution of each tape to the total inter-tape current sharing resistance (see figures 4), and calculates the resulting current and voltage distribution. The optimization approach iteratively varies the model input parameters to minimize the error between all simulated and experimental TITO experiments. A number of optimization formulations were prototyped and the following was determined to provide the best balance of simplicity and fit quality.

The optimization design vector is shown in equation (4), which consists of the 12 current sharing parameters and the termination resistance. A single termination resistance is applied by the inclusion of two variables; x_{term} and R_{term}. R_{term} is the magnitude of the termination resistance, and x_{term} is a continuous variable between 0–11 that is rounded to the single tape index to assign the termination resistance.

$$\vec{x} = < R_{\text{ct},L0T0}, \ldots, R_{\text{ct},L3T2}, x_{\text{term}}, R_{\text{term}} > \tag{4}$$

The goal is to find the single cable, defined by the percolation model with the parameters in equation (4), that provides the least squares fit to all of the TITO experiments. All input–output combinations are defined by figure 2 and listed below in table 2. Although all experimental combinations are considered, the optimization focuses only on the single transport current of 30 A, chosen as the highest case before some tapes exhibited a superconducting transition.

The optimization formulation is shown in equation (5). For each TITO experiment, the L2 norm is evaluated between all 12 measured tape voltages and the percolation-model simulated voltages using a given input vector $\vec{x}$. This error is then summed over all performed TITO tape combinations.

$$\min \sum_{\text{pairs}} ||\vec{V}_{\text{sim}}(\vec{x}) - \vec{V}_{\text{exp}}||_2 \tag{5}$$

We utilize the differential evolution algorithm [31] in Python, which is a variant of the genetic algorithm [32], to iteratively perturb the input variables $\vec{x}$ towards the error-minimizing cable parameters. The population-based nature of the algorithm is well-suited for parallelization, and the optimization process is computed across 56 processors of a PowerEdge c6520 server in the Lawrencium high performance computing cluster at LBNL. The differential evolution optimization is performed with a population size of 3600 designs over 300 iterations.

3. Results

3.1. Experimental measurements and uniform simulations

The amount of data produced in these TITO experiments exceeds what can be presented in a manuscript; readers are encouraged to see the supplemental results containing figures for all experiments in table 2.

Figure 5 shows the L0 T2 - L3 T2 experiment in a straight cable, where current is injected into the outer most layer and extracted from the inner most layer. The top left plot shows the measured voltage of each tape at 5, 10, 20, 30, 40, 50, 60 and 70 A. The horizontal black lines show the simulated voltage distribution using the percolation model with a uniform (and arbitrary) tape resistance of $20e-9[\Omega - m^2]$. The bottom right plot shows the simulated data, where the circle colors and circle text indicate the normalized voltage (0–1) and the line width and color indicate the normalized current. The bottom left plot shows the normalized measured voltages from the 30 A case in the top left plot. The top right plot shows the measurements of each tape as an *I*–*V* curve.

Figure 6 shows the L2 T0 - L1 T0 experiment with the cable bent to a 76 mm radius, where current is injected and extracted between the two middle layers. Although there are fewer resistive interfaces for current to flow through than figure 5, the measured voltages are lower. The simulated data are again produced using the same uniform contact resistivity as in figure 5, and (a) good qualitative agreement is seen between measurements and simulations.

The bottom-right plot shows the magnitude of the percolation effect discussed earlier in figure 3 for the trivial 4 node example. Although current is injected into L2 T0 and extracted from L1 T0, current also flows in the opposite direction (from layer 2 to layer 3) before flowing back into L2 T1 and L2 T2 in the same layer as the current injection tape L2 T0. The same effect is observed for the ground tape. Since these simulations consider uniform resistances, the voltage difference between any neighboring nodes is a proxy for the current distribution; for example, 1 A flows between input and output tapes (1.0–0.0), 0.33 A between the input tape and each of the tapes in layer 3 (1.0–0.667), et cetera. The simple percolation model can probe complex CORC® current sharing behaviors. Recall that the copper core is not considered in the TITO simulations.

Table 2 summarizes the input tape voltage of all TITO experiments for each cable radius at 30 A. In all experiments a significant reduction in voltage occurs when the cable is initially bent to a 152 mm radius, and further bending the cable to 76 mm results in further but diminishing reductions in voltage. The input voltage of tapes in layer 1 (neighboring outermost layer) were the most sensitive to bending. Considering the steep initial voltage drop with bending radius, the effect may be driven more by an increase in contact area than an increase in contact pressure. This would be a good topic for future work.

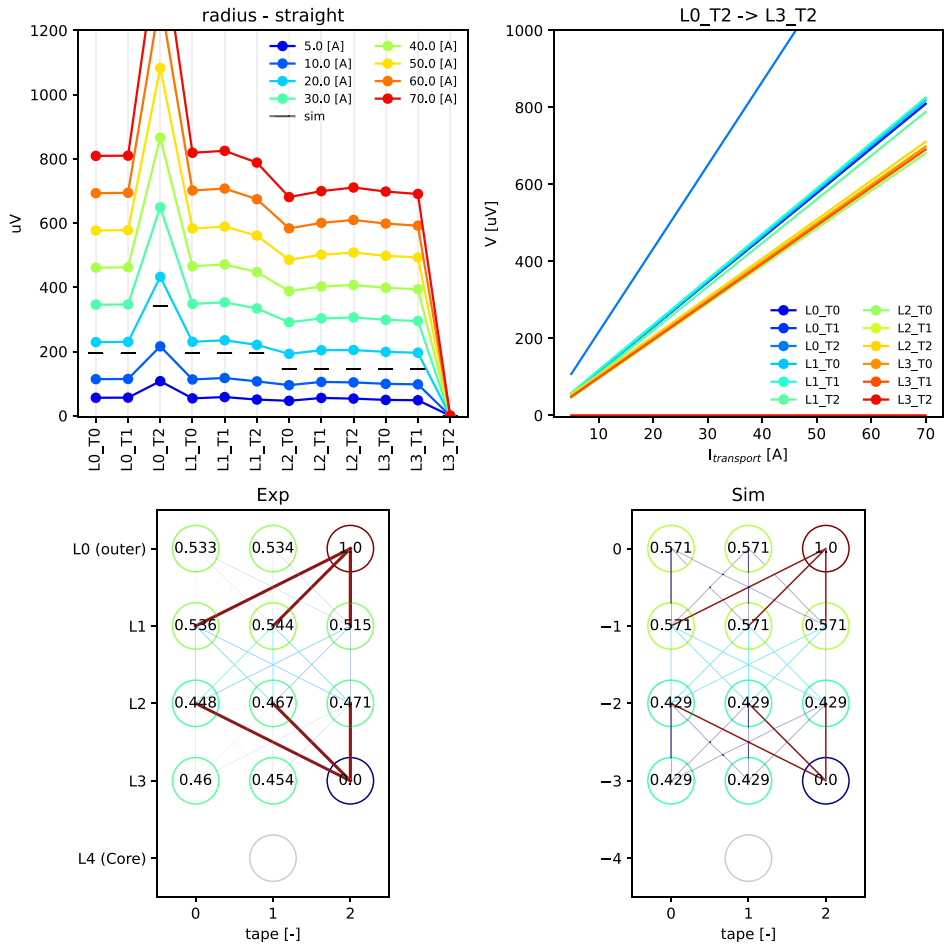

Figure 5. Measurement results for L0 T2 - L3 T2 (see figure 2) with a straight cable. Simulated voltage distributions (bottom right) here are with a uniform $R_{ct} = 20e-9[\Omega - m^2]$ assigned to each of the 12 tapes.

3.2. Simulations with extracted resistances

The optimization results are shown in figure 7 and summarized in table 3. The top plot shows the error-minimizing fit of the inter-tape contact resistance of each tape (x axis) and each cable configuration (straight, 152 mm and 76 mm radius). Recall that the total inter-tape contact resistance is the sum of the contributions of each tape. The inner-most layers (L3) have the highest inter-tape resistivities. The middle plot shows the same data as the top plot, but with each tape's resistivity normalized to the straight cable to highlight the relative change as the cable is bent. Layer 1 (second layer from outside) had the most significant reduction in resistance from bending, where the resistance of L1 T1 decreased by over 80 %. The bottom plot shows the resulting optimization fit of the termination resistance, where all three optimizations converged on L1 T2 as the potentially problematic tape in the experiments. The resistance values in all three cases (three separate optimization runs) are similar and are reported in table 4.

Figure 5 presents the straight cable results for current injection and extraction from the inner-most and outer-most layer using simulations with uniform resistances. Figures 8 and 9 show the same TITO pair but with the cable bent to 152 mm and 76 mm, respectively. Figures 8 and 9 also show the simulated results using the optimization-extracted parameters of tables 3–4, and a good agreement between the model and the 30 A experiment is observed. The top right plot here shows the I–V curve with the low-current linear fit removed, and a superconducting transition is observed in L0 T2. This tape had an elevated resistance in figure 7; if a local performance reduction exists inside the cable, the resistance fit may artificially increase as current shares over a reduced cable length.

Figure 10 shows a new TITO pair of L2 T2 - L3 T0, where good agreement is again observed between the 30 A experiments and simulations using the optimization-extracted parameters. A sharp superconducting transition is observed above 40 A in L2 T2. Figure 11 shows the I–Vcurves of only tapes L2 T1 (top) and L2 T2 (bottom) in the TITO experiment with an

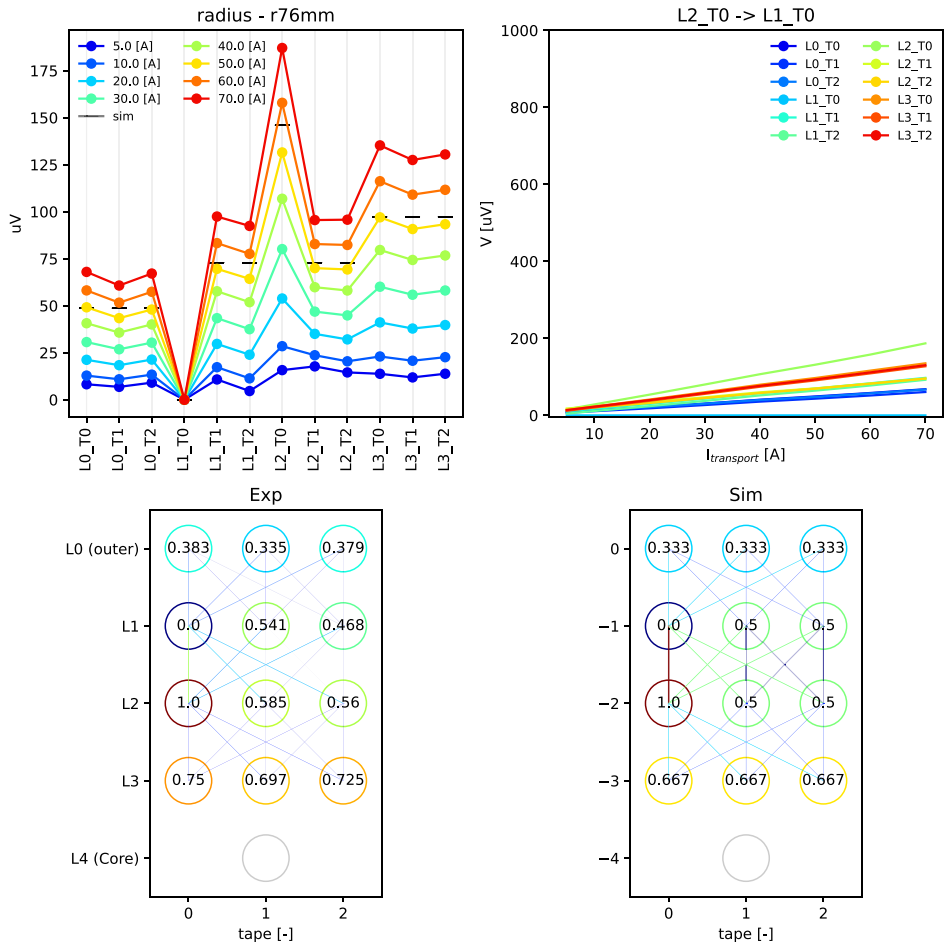

Figure 6. Measurement results for L2 T0 - L1 T0 (see figure 2) with cable bent to 76 mm radius. Simulated voltage distributions (bottom right) here are with a uniform $R_{ct} = 20e - 9[\Omega - m^2]$ assigned to each of the 12 tapes.

output tape L1 T0, where a superconducting transition is seen in each experiment. Bending a cable can introduce local tape performance reductions, which reduce performance and shift the *I*–*V* curve left toward lower critical currents [18]. Figure 11 shows the opposite effect, where bending the cable causes the *I*–*V* curve to move right toward higher currents as a result of the reduced inter-tape resistance. Bending the cable changed the cable operation and safe operating limits.

4. Discussion

This work presents an improved approach to measure and extract the inter-tape resistance in CORC® cables, allowing the inter-tape resistance of different tapes and layers to be resolved. An advantage of the TITO approach is the potential to obtain *in-situ*, near-real time cable data (e.g. sub-minute resolution). Although the automated TITO experiments and percolation model are very fast, the optimization process is not efficient and future work will work on faster parameter extraction techniques to be able to move the implementation towards real-time. With this same objective, future work will explore whether fewer TITO experiments can be performed while maintaining a high quality fit; for example, is a comparable result obtained by powering only the outer and inner most layers?

Our manuscript would benefit from the statistics of analyzing multiple CORC® cables. Since only a single cable was investigated, the results in table 3 should not be interpreted as a universal result for these conductors. The terminations in figure 1 are time consuming to implement, and developing a more efficient TITO termination is a priority for future work. On one hand, if the TITO transport currents are reduced, a number of TITO terminations concepts are possible with reduced implementation complexity. On the other hand, if TITO transport currents are increased and applied on both sides of the cable (i.e. further increasing implementation complexity from figure 1), the approach could potentially be expanded to probe tape superconducting transitions. In addition to the experimental challenges this would present, a fast HTS cable simulation tool would be required that can capture internal current redistribution around local tape defects. If achieved, this would approach an *in-situ* realization of the extracted tape measurements in Van der Laan (2024) [18].

Table 2. Input tape voltage for each TITO tape combination with $I_{\text{transport}} = 30$ A.

		V [μV]		
Input tape	Output tape	straight	$r = 152$ mm	$r = 76$ mm
L0-T0	L1-T0	232	76	68
L0-T0	L1-T1	248	61	55
L0-T0	L1-T2	350	206	201
L0-T0	L3-T0	480	203	185
L0-T0	L3-T1	514	200	178
L0-T0	L3-T2	515	204	179
L0-T1	L1-T0	263	74	63
L0-T1	L1-T1	233	62	57
L0-T1	L1-T2	382	210	201
L0-T1	L3-T0	497	204	184
L0-T1	L3-T1	532	201	178
L0-T1	L3-T2	532	205	178
L0-T2	L1-T0	365	229	180
L0-T2	L1-T1	354	220	167
L0-T2	L1-T2	506	359	310
L0-T2	L3-T0	614	358	296
L0-T2	L3-T1	649	355	290
L0-T2	L3-T2	649	359	290
L2-T0	L1-T0	196	82	80
L2-T0	L1-T1	173	62	60
L2-T0	L1-T2	298	202	201
L2-T0	L3-T0	315	153	143
L2-T0	L3-T1	346	157	137
L2-T0	L3-T2	349	157	141
L2-T1	L1-T0	204	84	84
L2-T1	L1-T1	193	63	65
L2-T1	L1-T2	322	205	207
L2-T1	L3-T0	342	179	161
L2-T1	L3-T1	384	174	160
L2-T1	L3-T2	378	176	152
L2-T2	L1-T0	181	79	81
L2-T2	L1-T1	174	60	63
L2-T2	L1-T2	302	202	206
L2-T2	L3-T0	333	172	161
L2-T2	L3-T1	367	164	150
L2-T2	L3-T2	369	173	153

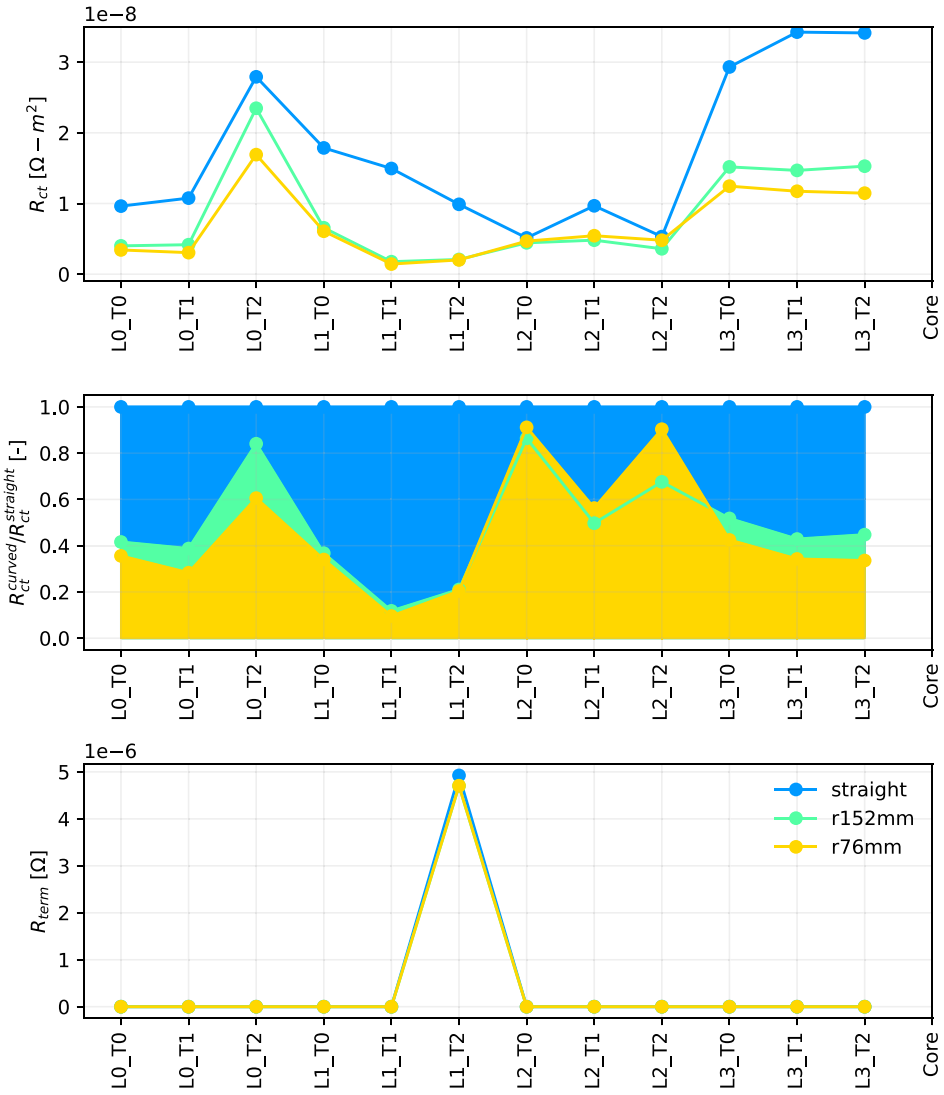

Figure 7. Optimization-extracted inter-tape and termination resistances. The inter-tape resistance between any two neighboring tapes is the sum of the two values reported in this figure (see figure 4 and accompanying text).

Table 3. Optimization-extracted inter-tape resistance from figure 7, supplementing results in table 4. The inter-tape resistance between any two neighboring tapes is the sum of the two values reported in this table (see figure 4 and accompanying text).

	R_{ct} [$n\Omega - m^2$]		
Tape	straight	$r = 152$ mm	$r = 76$ mm
L0-T0	9.6	4.0	3.4
L0-T1	10.8	4.2	3.0
L0-T2	27.9	23.5	16.9
L1-T0	17.9	6.6	6.1
L1-T1	15.0	1.8	1.4
L1-T2	9.9	2.1	2.0
L2-T0	5.1	4.4	4.7
L2-T1	9.7	4.8	5.4
L2-T2	5.3	3.6	4.8
L3-T0	29.3	15.2	12.5
L3-T1	34.3	14.7	11.7
L3-T2	34.1	15.3	11.5

Table 4. Optimization-extracted termination resistance fit from figure 7, supplementing results in table 3.

Configuration	Tape	R_{term} [$\mu\Omega$]
Straight	L1-T2	4.92
$r = 152$ mm	L1-T2	4.7
$r = 76$ mm	L1-T2	4.71

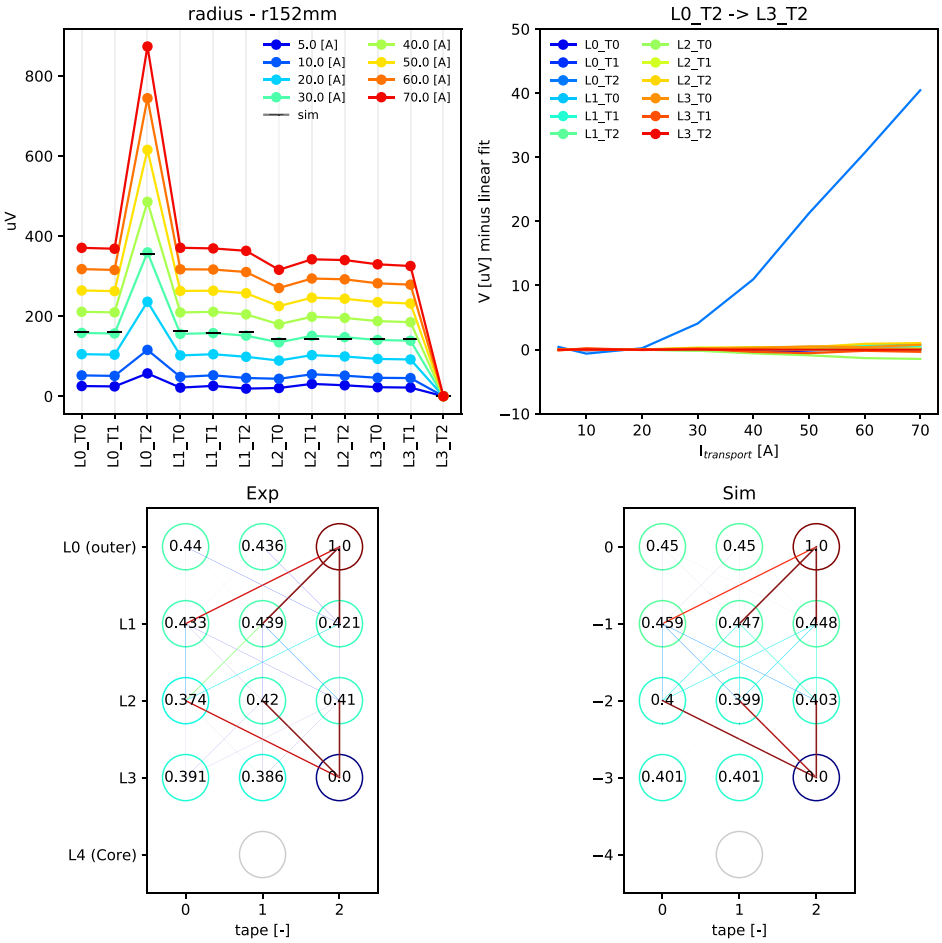

Figure 8. Measurement results for L0 T2 - L3 T2 (see figure 2) with the cable bent to a 152 mm radius. Simulated voltage distributions (bottom right) here are with the optimization-extracted parameters of tables 3 and 4.

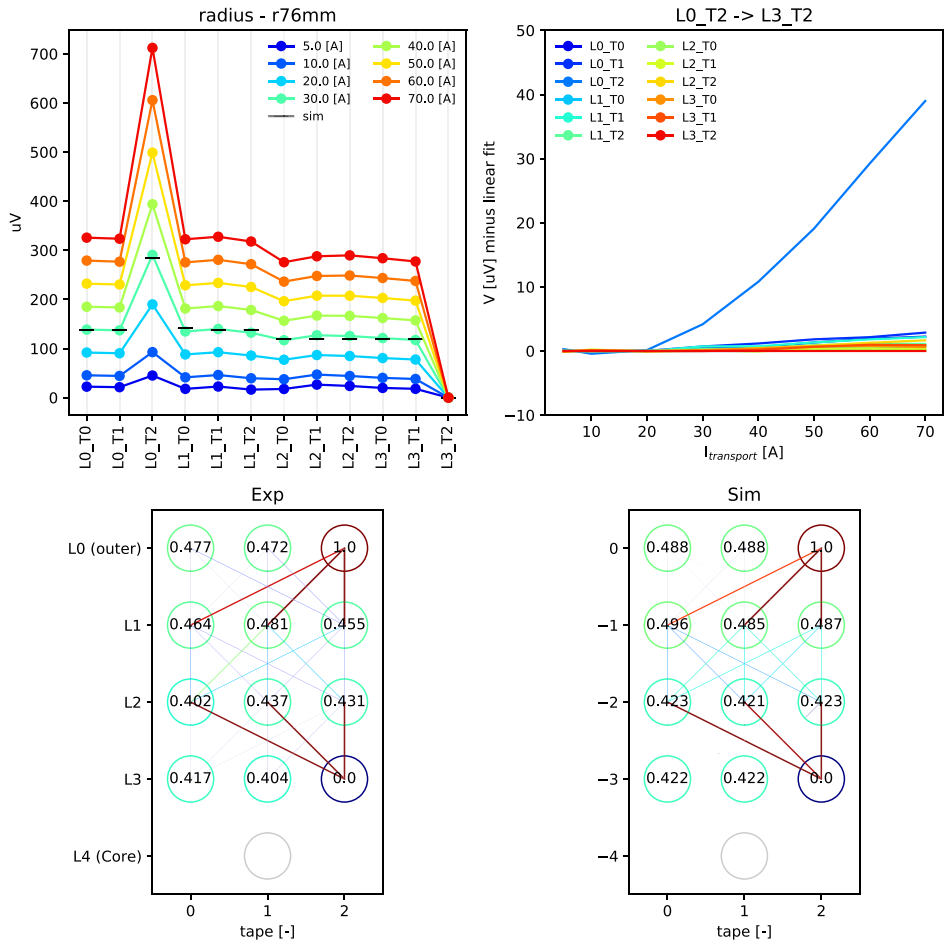

Figure 9. Measurement results for L0 T2 - L3 T2 (see figure 2) with the cable bent to a 76 mm radius. Simulated voltage distributions (bottom right) here are with the optimization-extracted parameters of tables 3 and 4.

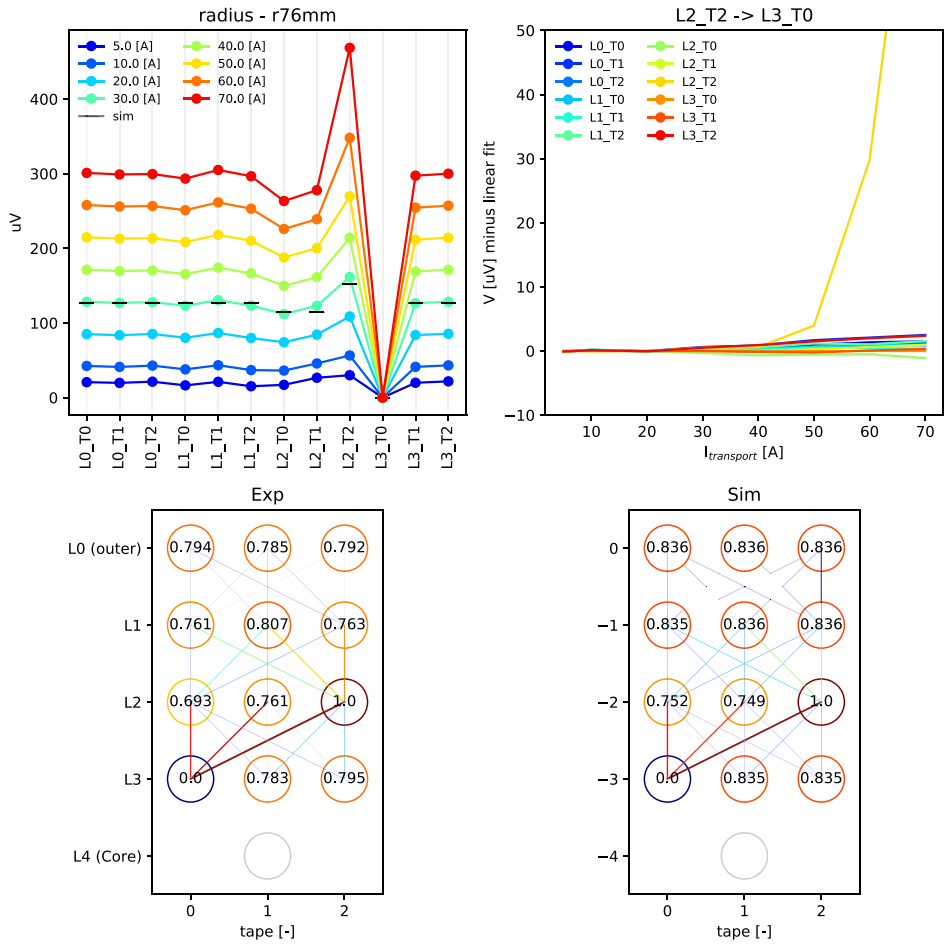

Figure 10. Measurement results for L2 T2 - L3 T0 (see figure 2) with the cable bent to a 76 mm radius. Simulated voltage distributions (bottom right) here are with the optimization-extracted parameters of tables 3 and 4.

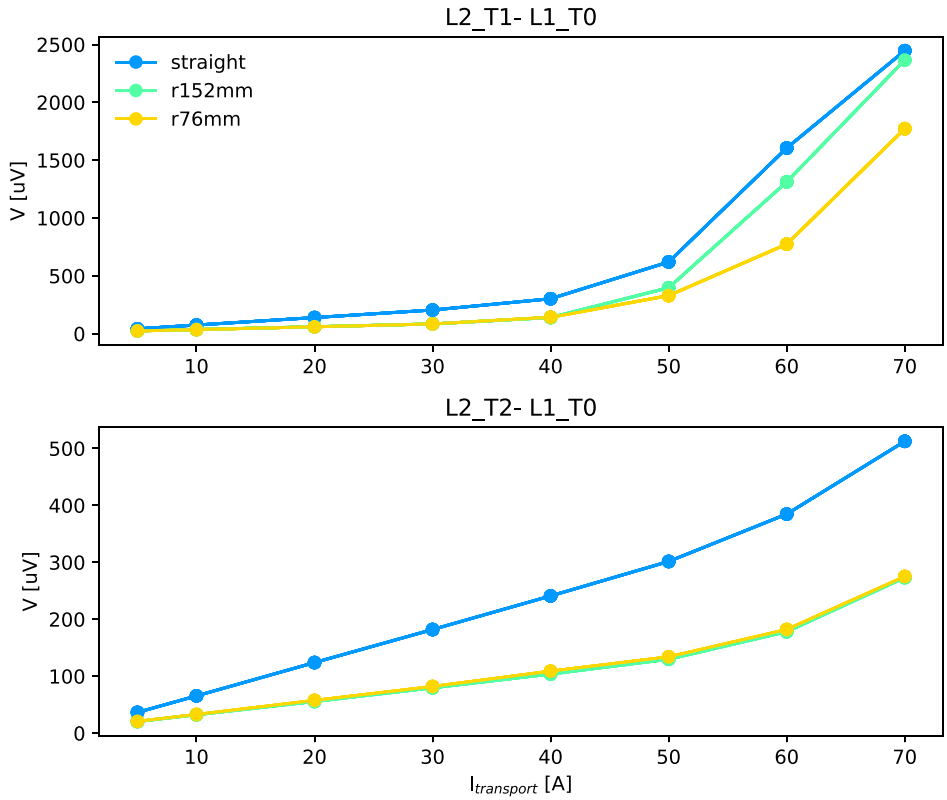

Figure 11. Selected TITO measurements (L2 T1 - L1 T0, top, L2 T2 - L1 T0, bottom) with tapes exhibiting superconducting transitions. The bent cables yielded lower voltages as a result of the decreased inter-tape resistance.

5. Conclusion

This work presents a new approach for resolving the local inter-tape resistances in CORC® cables, which is a key parameter behind the stability and performance limits of HTS cables. Developments in the cable termination, electrical controls for automated tape switching and a simplified model for current percolation in CORC® TITO experiments are presented. An optimization approach is utilized to fit a simplified model containing 12 contact resistance parameters to all TITO experiments, and the cable inter-tape resistances are presented as a function of layer and cable bending radius. The average inter-tape resistance decreases by more than 50% after bending the straight cable to a radius of 152 mm. Further resistance reductions when bent to a 76 mm radius are minimal. The inter-tape resistance of the outer-most layer is higher than internal layers, and the inner-most layer neighboring the copper core is more than 2–3 times more resistive than other tapes in the cable. Future work should decrease the implementation complexity of the TITO experiments to allow more cables to be tested, identify a more efficient optimization approach to facilitate *in-situ* monitoring, and intentionally probe tape superconducting transitions in addition to inter-tape contact resistances.

Data availability statement

The data that support the findings of this study are available upon reasonable request from the authors. Please see supplemental results PDF.

Acknowledgments

This work was supported by the U S Department of Energy, Office of Science, Office of High Energy Physics, through the US Magnet Development Program [5] under Contract No. DEAC02-05CH11231. This work was additionally supported by the U S Department of Energy, Office of High Energy Physics under Grant Numbers DE-SC0014009 and DE-SC0025836, and Office of Fusion Energy Sciences under Grant Number DE-SC0019934.

References

[1] Takayasu M, Chiesa L, Bromberg L and Minervini J V 2011 HTS twisted stacked-tape cable conductor *Supercond. Sci. Technol.* **25** 014011
[2] Uglietti D 2019 A review of commercial high temperature superconducting materials for large magnets: from wires

and tapes to cables and conductors *Supercond. Sci. Technol.* **32** 053001
[3] Laan D C V der, Weiss J D and McRae D M 2019 Status of CORC® wires cables and wires for use in high-field magnets and power systems a decade after their introduction *Supercond. Sci. Technol.* **32** 033001
[4] Hartwig Z S *et al* 2020 Viper: an industrially scalable high-current high-temperature superconductor cable *Supercond. Sci. Technol.* **33** 11LT01
[5] Prestemon S, Amm K, Cooley L, Gourlay S, Larbalestier D, Velev G and Zlobin A 2020 The 2020 updated roadmaps for the us magnet development program (arXiv:2011.09539)
[6] Coulter J Y, Holesinger T G, Kennison J A, Willis J O and Rupich M W 2009 Nondestructive investigation of position dependent ic variations in multi-meter coated conductors *IEEE Trans. Appl. Supercond.* **19** 3609–13
[7] Bykovsky N, Uglietti D, Wesche R and Bruzzone P 2018 Damage investigations in the HTS cable prototype after the cycling test in edipo *IEEE Trans. Appl. Supercond.* **28** 1–5
[8] Wang X *et al* 2020 Development and performance of a 2.9 Tesla dipole magnet using high-temperature superconducting CORC® wires *Supercond. Sci. Technol.* **34** 015012
[9] Xinbo H *et al* 2020 Analyses of the plastic deformation of coated conductors deconstructed from ultra-high field test coils *Supercond. Sci. Technol.* **33** 095012
[10] Xiao G Y, Liu F, Jin H, Zhou C, Qin J G, Liu H J, Li J G, Dai T L and Zhang X T 2020 Experimental study on cabling properties of different rebco coated tapes *J. Phys.: Conf. Ser.* **1559** 012111
[11] Ibekwe R T, Riva N'o, Whyte D G, Sanchez V J and Hartwig Z S 2024 A platform to study defect-induced behavior in high-temperature superconductor cables *Supercond. Sci. Technol.* **37** 085018
[12] Teyber R, Marchevsky M, Martinez A C A, Prestemon S, Weiss J and van der Laan D 2022 Numerical investigation of current distributions around defects in high temperature superconducting CORC® cables *Supercond. Sci. Technol.* **35** 094008
[13] Teyber R, Weiss J, Marchevsky M, Prestemon S and van der Laan D 2022 Current distribution monitoring enables quench and damage detection in superconducting fusion magnets *Sci. Rep.* **12** 22503
[14] Teyber R, Marchevsky M, Weiss J and van der Laan D 2022 A Halbach scanner for defect characterization in HTS cables *Applied Superconductivity Conf.* p 2LOr1D-05
[15] Weiss J, van der Laan D, Kim C H, Teyber R, Radcliff K, Phifer V, Davis D S, Zhang Y, Cooley L D and Pamidi S V 2025 Demonstration of current sharing around tape defects in a low-inductance CORC® wire solenoid generating a peak magnetic field of 4.6 T at 25 K *Supercond. Sci. Technol.* accepted (https://doi.org/10.1088/1361-6668/adedbd)
[16] Weiss J D, Teyber R, Marchevsky M and van der Laan D 2020 Quench detection using hall sensors in high-temperature superconducting CORC®-based cable-in-conduit-conductors for fusion applications *Supercond. Sci. Technol.* **33** 105011
[17] Marchevsky M 2021 Quench detection and protection for high-temperature superconductor accelerator magnets *Instruments* **5** 27
[18] van der Laan D, Weiss J, Radcliff K and Abraimov D 2024 CORC® wires allowing bending to 20 mm radius with 97.5% retention in critical current and having an engineering current density of 530 a mm− 2 at 20 t *Supercond. Sci. Technol.* **37** 115007
[19] Anvar V A *et al* 2018 Bending of CORC® cables and wires: finite element parametric study and experimental validation *Supercond. Sci. Technol.* **31** 115006
[20] Phifer V 2023 Experimental investigations of Tape-to-Tape contact resistance and its impact on current distribution around local IC degradations in CORC® Cables *PhD Thesis* (The Florida State University)
[21] Lai L, Zhao K, Yue Y and Chen G 2025 Design and prototype testing of a contactless HTS cable measurement system *Supercond. Sci. Technol.* **38** 045012
[22] Wang Y, Zhang M, Grilli F, Zhu Z and Yuan W 2019 Study of the magnetization loss of CORC® cables using a 3d TA formulation *Supercond. Sci. Technol.* **32** 025003
[23] Teyber R, Marchevsky M, Prestemon S, Weiss J and van der Laan D 2020 CORC® cable terminations with integrated hall arrays for quench detection *Supercond. Sci. Technol.* **33** 095009
[24] Halbach K 1980 Design of permanent multipole magnets with oriented rare earth cobalt material *Nucl. Instrum. Methods* **169** 1–10
[25] Jun L, Goddard R, Han K and Hahn S 2017 Contact resistance between two rebco tapes under load and load cycles *Supercond. Sci. Technol.* **30** 045005
[26] Bonura M, Barth C, Joudrier A, Troitino J F, Fete A and Senatore C 2019 Systematic study of the contact resistance between rebco tapes: pressure dependence in the case of no-insulation, metal co-winding and metal-insulation *IEEE Trans. Appl. Supercond.* **29** 1–5
[27] Jun L, Xin Y, Lochner E, Radcliff K and Levitan J 2020 Contact resistivity due to oxide layers between two rebco tapes *Supercond. Sci. Technol.* **33** 045001
[28] Yagotintsev K, Anvar V A, Gao P, Dhalle M J, Haugan T J, Laan D C V D, Weiss J D, Hossain M S A and Nijhuis A 2020 AC loss and contact resistance in rebco CORC®, roebel and stacked tape cables *Supercond. Sci. Technol.* **33** 085009
[29] Phifer V, Small M, Bradford G, Weiss J, van der Laan D and Cooley L 2022 Investigations in the tape-to-tape contact resistance and contact composition in superconducting CORC wires *Supercond. Sci. Technol.* **35** 065003
[30] Holm R 2013 *Electric Contacts: Theory and Application* (Springer)
[31] Storn R and Price K 1997 Differential evolution–a simple and efficient heuristic for global optimization over continuous spaces *J. Glob. Optim.* **11** 341–59
[32] Deb K, Pratap A, Agarwal S and Meyarivan T A M T 2002 A fast and elitist multiobjective genetic algorithm: NSGA-II *IEEE Trans. Evolutionary Comput.* **6** 182–97